University of Texas Rio Grande Valley

ScholarWorks @ UTRGV

Theses and Dissertations

12-2022

A Study of the Surface Properties of Additive Manufactured Inconel 718 After Laser Surface Treatment and CNC Grinding

Sampson K. Canacoo
The University of Texas Rio Grande Valley

Recommended Citation

Canacoo, Sampson K., "A Study of the Surface Properties of Additive Manufactured Inconel 718 After Laser Surface Treatment and CNC Grinding" (2022). *Theses and Dissertations*. 1126.
https://scholarworks.utrgv.edu/etd/1126

A STUDY OF THE SURFACE PROPERTIES OF ADDITIVE MANUFACTURED INCONEL

718 AFTER LASER SURFACE TREATMENT AND CNC GRINDING

A Thesis

by

SAMPSON K. CANACOO

Submitted in Partial Fulfillment of the

Requirements for the Degree of

MASTER OF SCIENCE IN ENGINEERING

Major Subject: Manufacturing Engineering

The University of Texas Rio Grande Valley

December 2022

A STUDY OF THE SURFACE PROPERTIES OF ADDITIVE MANUFACTURED INCONEL

718 AFTER LASER SURFACE TREATMENT AND CNC GRINDING

A Thesis
by
SAMPSON K. CANACOO

COMMITTEE MEMBERS

Dr. Anil Srivastava

Chair of Committee

Dr. Jianzhi Li

Committee Member

Dr. Farid Ahmed

Committee Member

December 2022

ABSTRACT

Canacoo, Sampson K<u>., A Study of the Surface Properties of Additive Manufactured Inconel 718</u> <u>after Laser Surface Treatment and CNC Grinding</u>. Master of Science in Engineering (MSE), December 2022, 44 pp., 10 tables, 24 figures, references, 46 titles.

This study investigated the surface properties of additive manufactured Inconel 718 produced through selective laser melting, and the effects of laser ablation and CNC grinding on the surface finish. The objectives were to investigate the effects of the various parameters of laser ablation and CNC grinding on the Inconel 718 surface. The parameters used for the laser experiments were pulse energy (4, 20, and 30 µJ), scanning speed (5, 10, and 15 mm/s), and hatch distance (10, 30, and 50 µm). For the grinding experiments, the wheel speed was kept constant at 20.3 m/sec, however, two different workpiece speed (8.6 and 14.7 m/min) and depths of cut (0.013 and 0.025 mm) were used. The average surface roughness of the samples were measured before and after the experiments, and the microstructure was also observed using scanning electron microscopy (SEM) and energy-dispersive spectroscopy (EDS). It was observed that laser ablation reduced the surface roughness, but there were cracks on the surface as a result of oxidation that occured during the process. On the other hand, the precision CNC grinding of the samples produced relatively better surface finish and also all the surface defects were eliminated.

DEDICATION

I dedicate this work to my family who have wholeheartedly supported me all my life, especially in this journey to accomplishing this degree.

ACKNOWLEDGMENTS

I am grateful to Dr. Anil Srivastava, the chair of my thesis committee, for all his guidance and support. I am also very grateful to Dr. Jianzhi Li and Dr. Farid Ahmed for their advice and direction on my project to ensure its successful completion.

TABLE OF CONTENTS

LIST OF FIGURES

CHAPTER I

INTRODUCTION

Inconel 718 is a nickel-based alloy with applications in aerospace, nuclear power plants, gas turbines and a wide range of high temperature applications [1]. The alloy has been used in these areas because it possesses excellent fatigue resistance, corrosion resistance, good weldability and can maintain its high strength at elevated temperatures of up to 650 ℃ [2]. These properties also make Inconel 718 difficult to machine using traditional manufacturing processes. The manufacturing process of Inconel 718 is costly because the low thermal conductivity of the alloy, which allows it to withstand high temperatures, causes heat concentration at the tool tip during machining processes. This leads to accelerated tool wear and deterioration, increasing tooling costs. An alternative solution to produce Inconel 718 components more effectively is selective laser melting (SLM) additive manufacturing.

Additive manufacturing allows the production of complex shapes without the limitations associated with traditional manufacturing. SLM is a process that involves using a high-power laser to selectively melt and fuse metallic powders layer by layer until a 3D object is produced according to the CAD model of the object [3]. In general, additive produced parts have high surface roughness, porosity, balling effects, hatch marks, and cracks which are caused by the layer-by-layer construction process [4], [5]. Post processing is necessary to remove these defects from the surface of additive manufactured parts. There are several ways to treat the surface of additive

manufactured metal to improve the surface integrity. In this research, laser treatment and traditional grinding are considered.

Limited literature exists on the use of femtosecond laser ablation to improve the surface of selective laser melted Inconel 718. A good amount of literature focuses on the use of microsecond, picosecond, and nanosecond lasers for surface improvement through laser polishing. To study the performance of femtosecond laser ablation, the results were compared to CNC grinding which is widely used in industry.

Research Questions

The research aims to improve the surface quality of Inconel 718 part developed using additive manufacturing. The following research questions have been presented as a basis for our research:

1. What is the relationship between laser ablation parameters and the surface properties of selective laser melted Inconel 718?

2. What is the relationship between grinding parameters and the surface properties of selective laser melted Inconel 718?

3. How are the surface properties of Inconel 718 samples treated by grinding and laser ablation comparable to each other?

CHAPTER II

LITERATURE REVIEW

Selective Laser Melting

Selective laser melting is an additive manufacturing technique that involves applying laser beam scans at a controlled speed to specific positions on a powder bed to melt and fuse the powder into a solid material. After the desired cross-section is achieved for one layer, the powder bed is lowered by the set layer thickness and a new layer of powder is spread evenly across the powder bed [6]. The process is repeated until the part is complete. The build chamber is filled with an inert gas, typically argon or nitrogen to prevent oxidation during printing [7].
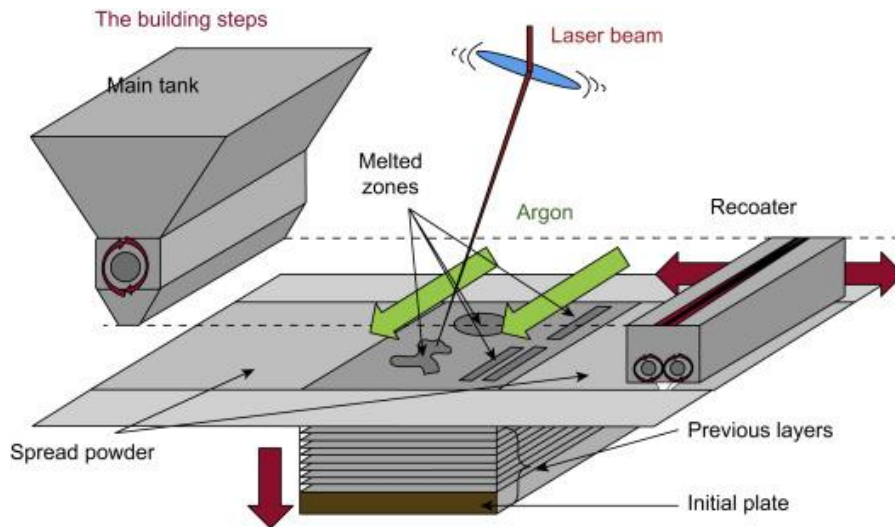
Figure 1: Selective Laser Melting diagram [8]

Additive manufactured parts typically do not possess the desired surface finish and mechanical properties required for certain applications [4]. In selective laser melting, several defects occur in the metal due to the rapid solidification of the metal powder after being melted by the laser, as well as the layer-by-layer nature of the process. These defects include porosity, cracks, balling, and hatch marks, and staircase effect [5], [9].

Porosity consists of spaces within the fused material part. The spaces are found between adjacent layers or within the layers themselves. The spaces within the layers are known as 'acicular pores' and are the most common pores that occur in a part [10]. Pores appear in different sizes and shapes and are caused by the large thermal gradients that occur due to the repeated rapid melting and solidification [11]. Porosity strongly affects the fatigue performance and crack growth characteristics of the part [12].

Cracking occurs due to thermal residual stresses in the selected laser melted part [13]. Two distinct mechanisms, the temperature gradient mechanism and the cool-down phase of molten top layers, are responsible for residual stresses [14]. If the tensile stress surpasses the ultimate tensile strength of the solid material, stress release occurs through fracture. Solid phase cracking is also referred to as hot cracking [15]. Delamination is another type of cracking in which cracks start between parallel layers. When residual stresses are greater than the capacity of two layers to bind together, this occurs [16], [17].

Balling occurs when the metal cools down into round balls instead of flat solid layers [18]. This is caused by surface tension, which prevents the molten metal from wetting the layer below it. The balling effect increases roughness of the surface and causes the occurrence of large number of pores between layers of discontinuous metal balls [19].

Several experiments have been carried out to reduce the surface roughness and defects on Inconel 718 and other high strength alloys using laser treatment and grinding wheel. Previous results are summarized and presented as follows.

Laser Polishing

Laser surface treatment is a non-contact, highly efficient way to reduce surface roughness. In laser polishing, the liquid in the molten pool is redistributed to the same level by gravity and surface tension after the laser melts the material's surface. The surface roughness is then minimized as the liquid hardens [20].
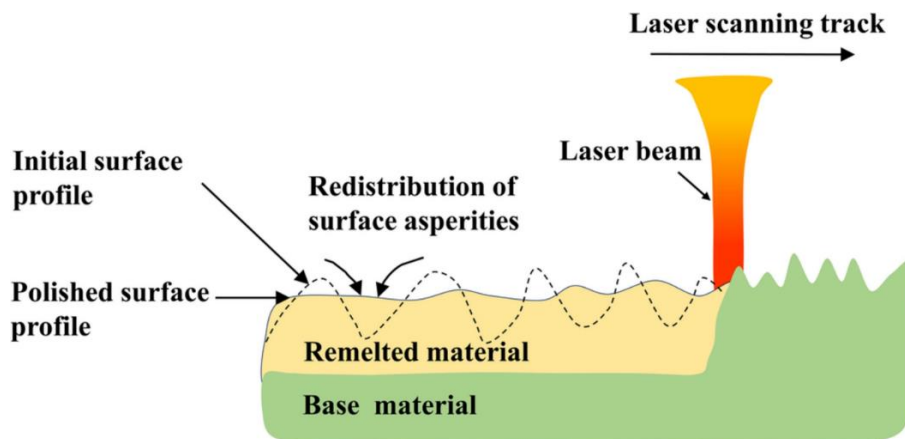
Figure 2: Laser polishing [21]

Zhihao et al. [22] used a nanosecond pulsed fiber on a flat Inconel 718 sample with a length of 50 mm, width of 50 mm and a height of 5mm. The surface roughness Ra decreased from 7.5 μm to below 0.1 μm, and Rz decreased from 31 μm to 0.6 μm. The microhardness of the surface increased from 345HV to 440HV.

Dadbakhsh et al. [23] improved the surface finish of LMD Inconel 718 samples using laser polishing at different parameters. They came to the conclusion that surface roughness may be

efficiently reduced to below Ra of 2 μm, which is roughly 80% less than the initial roughness, using a laser with a power of 500 W and a speed of 800-850 mm/min.

Guoqing et al [24] investigated the surface properties of Inconel 718 after laser polishing. The rough surface of selective laser melted IN718 was polished with a nanosecond fiber laser. The laser had a 1064 nm wavelength, a 1 mJ pulse energy, and a 50 μm spot size. The parameters for the pulse width, repetition frequency, scanning speed, and overlapping ratio were set to 220 ns, 20 kHz, 70 mm/s, and 90%, respectively. The surface roughness Ra and Rz were 8 μm and 33 μm before polishing, and they afterward dropped to 0.2 μm and 0.8 μm, respectively. The wear resistance and corrosion resistance also improved.

Yilbas et al. [25] analyzed the thermal stress of Inconel 718 after laser surface treatment. A CO_2 laser with a focal length of 127 mm and a nominal output power of 2 kW was utilized to irradiate the workpiece. At the surface of the workpiece, the laser beam's diameter was 0.3 mm. Nitrogen was the shielding gas that was used. The temperature and stress were predicted using a finite element model. The material changes in the laser irradiated region were examined using SEM, optical microscope, and XRD. They saw a sharp temperature decline, especially inside the workpiece, around the irradiated region. Low Von-Mises stresses were found in high-temperature regions, while high values were found in areas with sharp temperature decay. It was predicted that the residual stress would be within the alloy's yielding limit. SEM micrographs demonstrated the absence of microcracks on the surface. At the surface, the microhardness increased. The laser-treated area was about 50 μm below the surface.

Yilbas et al. [26] investigated the surface characteristics of Inconel 718 after laser treatment. The workpiece surface was irradiated using a CO_2 laser with a 2kW output power operating in pulse mode at various frequencies. The focusing lens had a 127 mm nominal focal

length. At the workpiece surface, the laser beam's diameter was 0.3 mm. The assisting gas employed was nitrogen. In the trials, Inconel 718 samples measuring 15 mm by 10 mm by 3 mm were employed. Measurements were taken of the laser-treated surface's microhardness, residual stress, and friction coefficient. The laser-treated surface was discovered to be free of significant defects such as cracks and voids. The laser treated area was approximately 20 μm thick below the surface. The surface residual stress was compressive in nature. At the laser-treated surface, the friction coefficient is lower than at the untreated surface. Surface hydrophobicity was enhanced after the laser treatment.

Li et al. [27] analyzed the thermodynamics and rapid solidification of laser polished Inconel 718. Inconel components were fabricated in an EOSINT-M280 DMLS system. The specimens were polished under argon using a nanosecond pulsed fiber laser with the following specifications: wavelength 1064 nm, pulse duration 150 ns, repetition rate 300 kHz, scanning speed 230 mm/s, overlapping ratio 40%, spot size 50 μm. The average roughness reduced from Ra exceeding 10 μm to below 0.1 μm. The surface porosity decreased by 65.7%. There were no shrinkage cavities, pores and microcracks.

Laser Ablation

Laser ablation is another application of laser to improve the surface characteristics of additive manufactured parts. In laser ablation, the material under laser irradiation absorbs laser energy, and is heated to melting temperature, and subsequently to vaporization temperature leading to the removal of material [28].
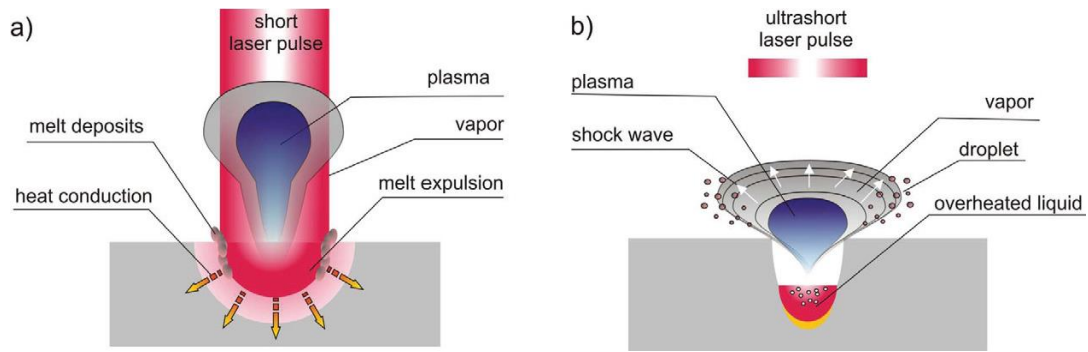
Figure 3: Laser ablation process [29]

Mohammad et al. [30] investigated the effect of laser ablation parameters on surface improvement of Ti-6Al-4V alloy sample produced using electron beam melting. A range of laser fluences were applied on the surface. The finest possible surface finish obtained was a roughness of about 13 μm, which was about 60% reduction.

Campanelli et al. [31] investigated laser ablation on selective laser molten steel parts, and the optimization of the surface finish through the process. The Taguchi method was used to identify the ideal process parameters for minimizing surface roughness. They discovered that the surface finish was impacted by the faster scan speeds. To optimize roughness, the laser power and repetition rate had to be set to their maximum values. Kruth et al. [32] used optimized parameters for laser erosion to reduce the roughness of SLM CL20ES stainless steel from Ra of 15 μm to 6 μm, which was a 60% reduction.

Grinding

Grinding is an abrasive process that involves material removal when a grinding wheel encounters the workpiece. Each active grain on the wheel surface removes a chip from the surface of the workpiece and provides average surface finish [33]. Grinding is still one of the main operations required for completing the machined components, despite the rapid development of

8

unconventional machining methods. [34]. It is also used as a post-processing method for finishing additive manufactured parts because it provides required surface finish, dimensional accuracy along with high tolerances that are needed in many industry applications.
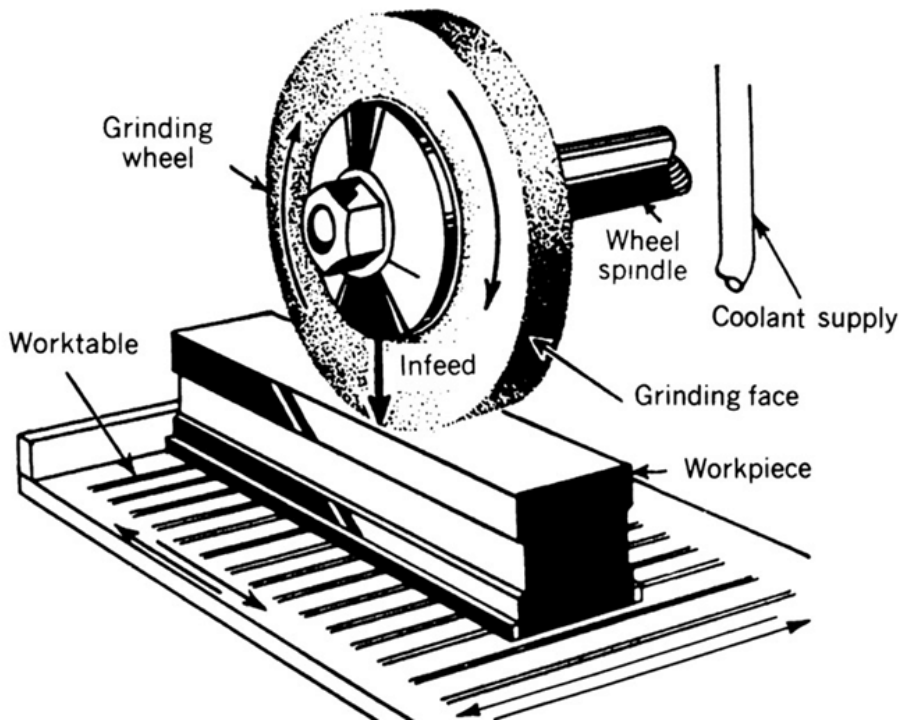
Figure 4: Grinding process [35]

A number of investigations have been performed on the grinding of Inconel 718 or high strength alloy components produced by laser sintering or traditional machining.

Tso [36] studied grinding of Inconel 718 using a KENT KCF-52 NC-type surface grinder with variable wheel speed and down-feed controls. Grinding wheels with different specifications, namely, WA46K8V, GC60J8V and CBN100P754 were used. The attrition wear and chip types were observed using a microscope. For Inconel 718, it was found that surface roughness rises with decreasing wheel speed and down-feed. Surface roughness using down-grinding was observed to be better than up-grinding. The GC60J8V grinding wheel was better suited to dry grinding. Due to its high stiffness, the CBN grinding wheel possessed the best dimensional precision. Based on

grinding force, dimensional accuracy, surface roughness, and grinding wheel life, it was determined that the CBN grinding wheel was best for grinding Inconel 718.

Novak et al [37] analyzed the surface profile after grinding Inconel 718 alloy. Specimens were ground in experiments under various conditions, and the roughness, as well as the Material Ratio Curve (Abbott Firestone Curve), were observed. 12 samples were ground with a silicon carbide grinding wheel. A semisynthetic process liquid in a 5% aqueous solution was used as the cutting fluid. The experiment included both longitudinal and grooving grinding techniques. They discovered that the best profile and Material ratio curve were obtained by longitudinal grinding at a cutting speed of 45 m/s and a feed rate of 0.04 m/min.

Wang et al [38] investigated the surface corrosion behavior of Inconel 718 after robotic belt grinding. Electrochemical testing in a 3.5 wt% NaCl solution at room temperature was used to determine this. The robotic belt grinding system used a specific Al_2O_3 abrasive belt that was placed on an elastic paper strip with reinforced fibers. The prepared specimens were processed using a belt at a speed of 21 m/s and a grinding force of 178 kPa. Three distinct belt types with three different particle sizes – 500, 178, and 125 μm were chosen. The specimens were divided based on their surface roughness, residual stresses, and morphology. They came to the conclusion that decreasing surface roughness and residual stress increases the specimen surface's corrosion resistance.

Yao et al [39] investigated the surface integrity of Inconel 718 after grinding using a resin cubic boron nitride (CBN) wheel and a vitrified bond single alumina (SA) wheel. By using both types of wheels, the effects of various grinding parameters on grinding temperature, grinding force, and grinding chip characteristics were examined. Investigations were also conducted on the workpiece's topography and surface roughness after utilizing SA and CBN wheels. They found

10

out that with increase in workpiece linear speed or depth of cut, grinding force and temperature increase. Using a single alumina wheel with a grinding depth of 0.005 mm, workpiece linear speed of 16 m/min, and wheel linear speed of 5 m/s achieved a better surface finish and was more suitable for grinding Inconel 718.

Srivastava and Pavel [40] investigated the effects of various grinding parameters on the surface integrity of titanium Ti-6Al-4V alloy parts produced using direct metal laser sintering (DMLS) process. According to the findings of their experiments, low stress grinding parameters should fall between the ranges of 10.2 m/s and 20.3 m/s for wheel speed, 12 m/min to 14.7 m/min for feed rate, and less than 0.025 mm for depth of cut. To prevent tensile residual stresses in ground sections, the combination of these factors should result in an equivalent chip thickness of less than 0.254 mm and a specific material removal rate of less than 4.3 mm^3/s/mm. Focusing on the surface integrity for both the surfaces with compressive and tensile residual stresses, the microstructure was examined. The material that may have been plowed over by the abrasive grits was visible on both types of surfaces, but it was more evident on surfaces with tensile residual stresses. They evaluated the residual stresses produced during the grinding of DMLS Ti-6Al-4V and conventional Ti-6Al-4V samples. The DMLS Ti-6Al-4V samples with only compressive stresses produced slightly superior results.

The effects of grinding wheel specifications on surface integrity and residual stress when grinding Inconel 718 were studied by Curtis et al [41]. They came to the conclusion that Inconel 718 component distortion was influenced by wheel technology. A distinct difference between diamond and CBN was observed when examining super abrasive wheel technology. Compressive residual stress states were accomplished by diamond wheels over CBN. Increasing aggression in

manipulating grinding parameters with CBN abrasives was associated with higher tensile stress regimes and distortion magnitudes.

CHAPTER III

MATERIALS AND METHODS

This chapter presents the materials used and steps that were followed to answer the research questions of this thesis.

Femtosecond Laser Ablation Study

An experiment was carried out to investigate the femtosecond laser ablation process to improve the surface of SLM Inconel 718 by varying pulse energy, scanning speed, and hatch distance. The performance measure for this investigation was surface roughness (Ra). The optimal process parameters were found using statistical analysis.

Experimental Setup

The laser used for the laser ablation study was a Spectra-Physics Spirit One Laser. The laser system delivers a pulse energy of up to 40 µJ at a repetition rate of 200 kHz, and an output of 1040 nm. The pulse width is 400 fs.

Figure 5: SLM printed Inconel 718 samples

Inconel 718 samples ($10 \times 10 \times 10$ mm) were manufactured using SLM. The composition of the as received Inconel 718 powder used is shown in Table 1. The surface roughness of all the faces of the samples were measured, and the roughness average Ra was 13.04±0.5 µm.

Table 1: Composition of Inconel 718 powder

Element	Ni	Cr	Fe	Nb	Mo
%	52.34	18.22	Balance	4.8	2.94
Element	Ti	Al	Co	C	Mn
%	0.34	0.41	0.7	0.04	0.20
Element	Si	P	S	B	Cu
%	0.012	0.09	0.05	0.05	0.25
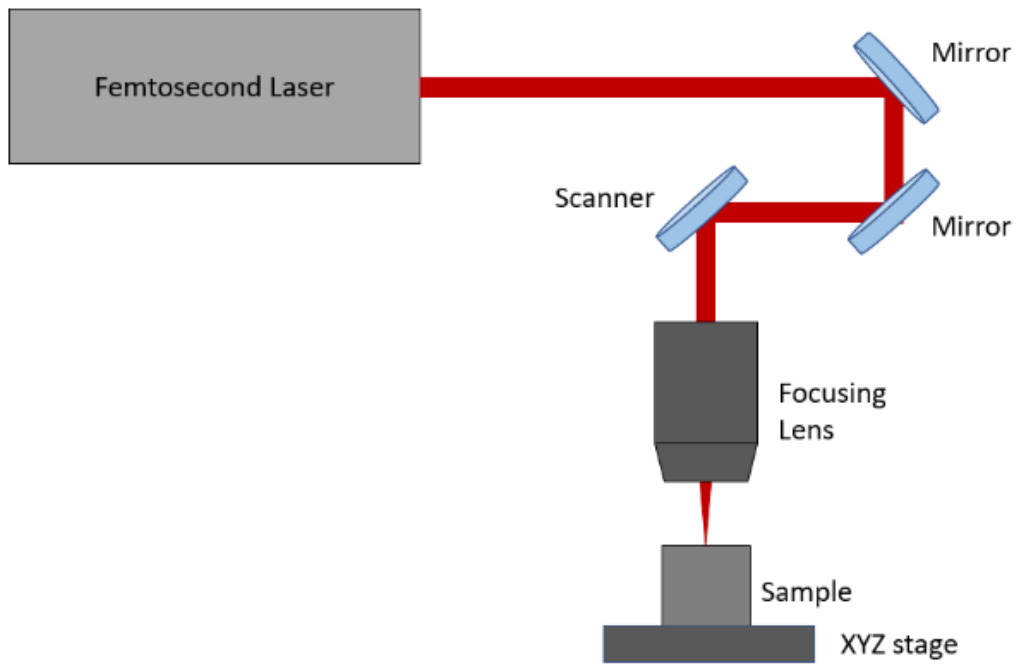
Figure 6: Schematic of femtosecond laser system
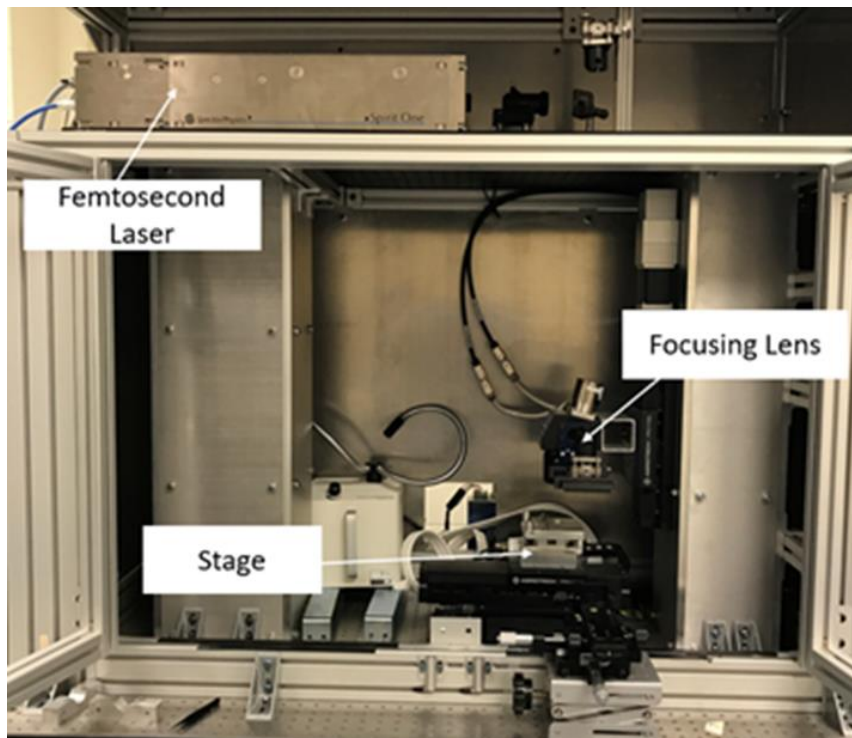
Figure 7: Laser ablation experimental setup

Focal Length Selection

Before the laser ablation experiment was run, a test was conducted in order to select the appropriate focal distance of the laser system to match the height of the printed samples. Using the right focal distance ensures that the focal point of the laser falls exactly on the surface of the sample. The focal point is the point at which the laser beam diameter is the smallest. Laser fluence is defined as laser energy per unit area, therefore the smaller the incident diameter of the laser beam on the surface, the larger the fluence, and more material is removed. The focal length of the system was altered by changing the z-value in the g-code. The effect of the z-values was tested by applying single pulses on the IN718 surface with a pulse energy 40 µJ and z-values ranging from 114.5 mm to 114.95 mm with 50 µm increments between them. The craters produced by the pulses were observed and measured using the microscope. The depths of the craters were measured, and z-value of 114.8 mm was selected, because it produced the crater with the smallest diameter of 20.61 µm and the largest depth of 92.81 µm.
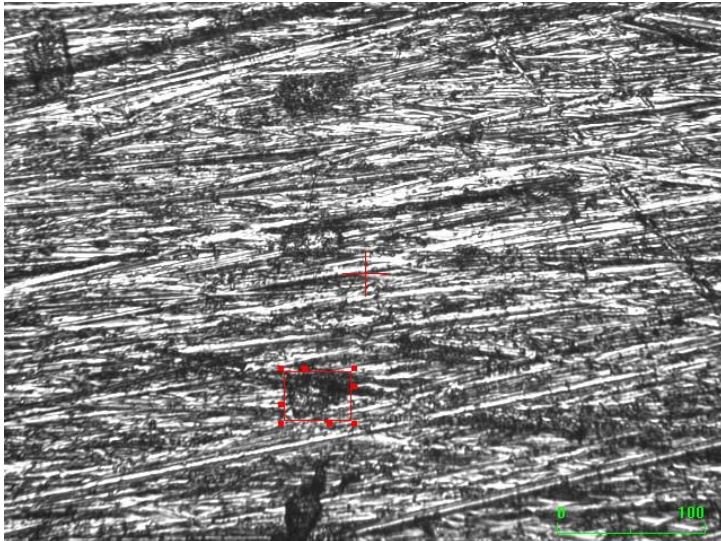
Figure 8: Craters on sample surface produced by laser pulses

Femtosecond Laser Ablation

Three laser parameters were selected for this laser ablation study with three levels. The variables are pulse energy, scanning speed, and hatch distance. These parameters were selected based on literature and the results from previous experiments. Table 2 shows the parameters and their various levels. A full factorial experiment was used, with 3 replicates of each combination of the processing parameters. The laser ablation was applied on 3 x 6 mm areas on the vertical surfaces of the SLM samples. Figure 9 shows the scanning strategy that was applied. After the experiment, the surfaces of the samples were observed using a VHX 5000 microscope and the surface roughness average Ra was measured using a Mahr M 300 C profilometer. Three Ra measurements were taken on each sample and the average value was recorded.

Table 2: Laser parameters with levels

Parameters	Levels		
Laser Energy (µJ)	4	20	36
Scanning Speed (mm/s)	5	10	15
Hatch Distance (µm)	10	30	50
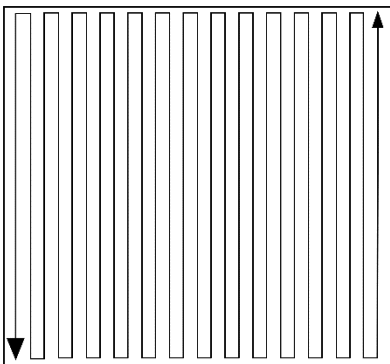
Figure 9: Laser scanning strategy

Precision CNC Grinding Study

A precision CNC Grinding study of additively manufactured Inconel 718 samples was carried out to investigate the effect of grinding process parameters (grinding wheel speed, feed rate and depth of cut) on the ground surface integrity. In this regard, few selected grinding tests were conducted using additively manufactured Inconel 718 samples and surface integrity of the ground samples were studied.

Experimental Setup

The investigations were performed using a Precision CNC Surface Grinding Machine (SUPERTEC, MASTER-1632CNC-3AXIS-FANUC) shown in Figure 8. This machine includes extremely precise vertical linear guide ways coupled with extra-large slide blocks to significantly increase spindle rigidity. Feed unit settings can be customized to 0.001mm using a vertical servo motor and precision ball screw. The patented control panel significantly improves operational comfort. The precision ball screws drive on the CNC three axes servo motor enhances productivity and positioning accuracy. Additionally, user-friendly CNC control increases overall efficiency. By turning a knob, the variable longitudinal travel speed is simply and readily regulated. The control has been built with distinctive safety features. Figure 9 shows the sample clamped in a vice inside the grinding machine.

Figure 10: Supertec CNC Grinding Machine
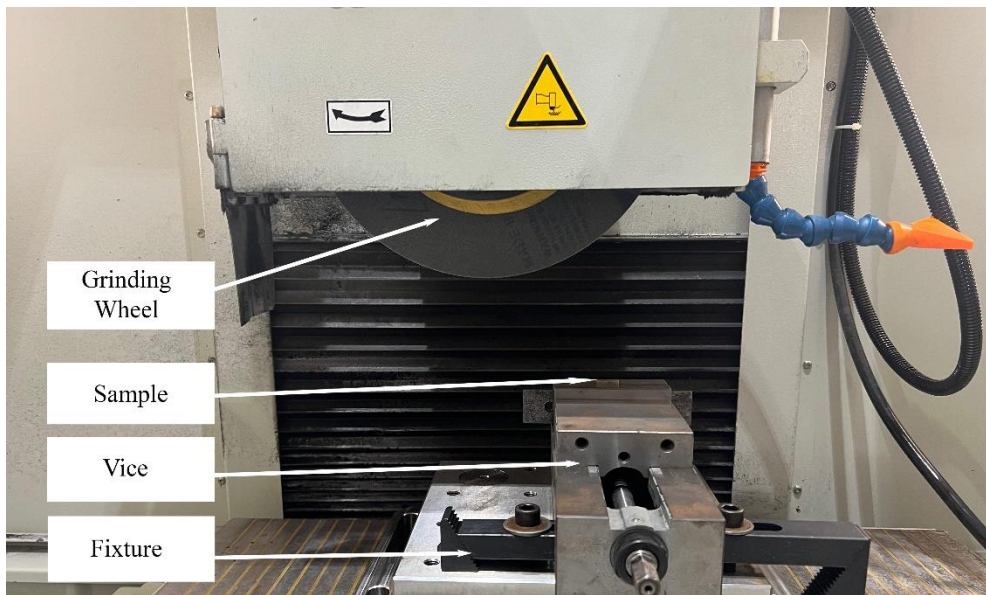
Figure 11: Sample setup

The Inconel 718 samples dimensions were 20×10×5 mm that were produced using selective laser melting (SLM) using an EOS M 290 Printer. The side with a width of 5 mm was ground. This is because the part was printed with the 5 mm as the height so the effect of the

layer-by-layer building process on the surface roughness was observed the most on those sides.

Two grinding wheels having Vitrified bond were used for the grinding tests. Vitrified bonded

wheels are used for precision grinding. Both of these Al_2O_3 grinding wheels were 12-inch in

diameter, one having grit size of 46, hardness 'H', coarse grade and the other having grit size of

60, hardness 'K', and medium grade. The surface roughness of the samples were measured

before and after grinding using a Mahr M 300 C profilometer. Three Ra measurements were

taken on each sample and the average value was recorded.

Ground surface

build
direction

5 mm

20 mm

10 mm
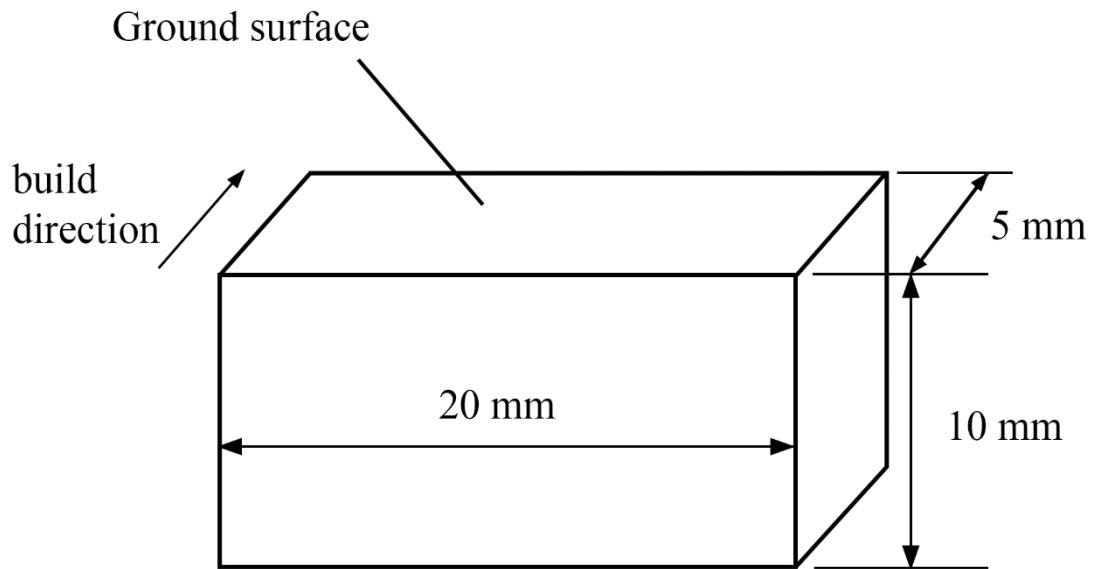
Figure 12: Specimen size and ground surface
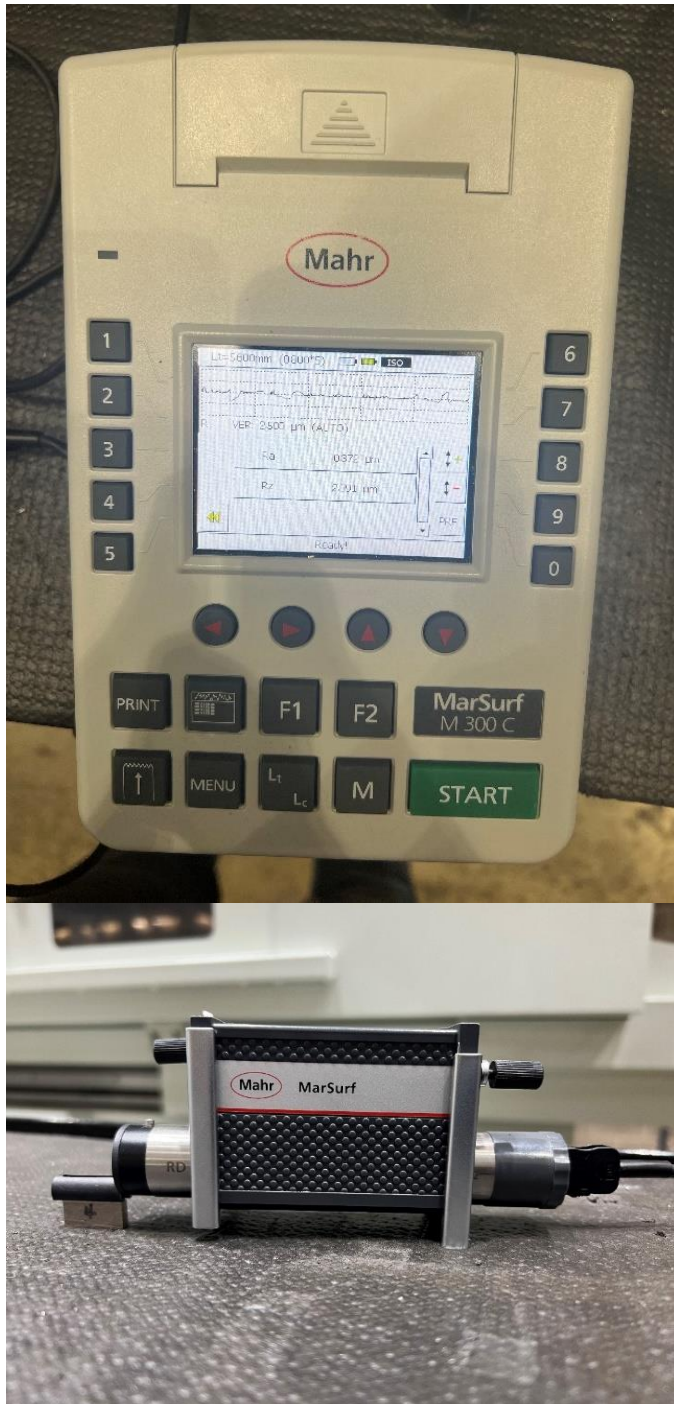
Figure 13: Mahr M300C profilometer probe on sample measuring surface roughness

The wheel specifications and parameters for grinding experiments are given in Table 3 and 4, respectively.

Table 3: Wheel Specifications

Wheel Number	Specifications/ Details
1	Aluminum Oxide, Grit size of 46, H hardness, Coarse Grade, Vitrified Bond
2	Aluminum Oxide, Grit size of 60, K hardness, Medium Grade, Vitrified Bond.

Table 4: Parameters for Grinding Experiment

Wheel speed, v_s (m/s)	Workpiece speed, v_w (m/min)	Depth of cut, a (mm)
20.3	8.6	0.013
20.3	14.7	0.025

Characterization Techniques

After the laser ablation and the CNC grinding experiments, the microstructures of the samples were analyzed using a Carl Zeiss SigmaVP Scanning Electron Microscope (SEM) and an EDAX Octane Super Energy Dispersive X-Ray Spectroscopy system (EDS).

Hardness Test

The hardness of the samples before and after laser ablation and CNC grinding were measured using a Wilson Hardness Rockwell 574 tester. A C diamond identer was used with a load of 100 kgf and a dwell time of 5 sec. An average of 4 indentations was made to each sample.

Figure 14: Wilson Hardness Rockwell 574 tester

CHAPTER IV

RESULTS AND DISCUSSION

Surface Roughness Analysis

Laser Ablation

After the laser ablation experiments, the surface roughness averages of the samples were measured. The lowest roughness average recorded was Ra of 3.098 µm. To observe the significance of each laser ablation parameter on the surface roughness, an analysis of variance was performed using Minitab Statistical Software. Table 4 shows the results of the ANOVA.

Table 5: ANOVA results

Source	DF	Adj SS	Adj MS	F-Value	P-Value
Model	18	80.105	4.4503	28.38	0.000
Linear	6	70.628	11.7713	75.06	0.000
Pulse Energy	2	14.481	7.2404	46.17	0.000
Scanning Speed	2	9.279	4.6394	29.58	0.000
Hatch Distance	2	46.868	23.4341	149.44	0.000
2-Way Interactions	12	9.477	0.7897	5.04	0.000
Pulse Energy*Scanning Speed	4	5.976	1.4941	9.53	0.000
Pulse Energy*Hatch Distance	4	1.638	0.4095	2.61	0.044
Scanning Speed*Hatch Distance	4	1.863	0.4656	2.97	0.026
Error	62	9.723	0.1568		
Lack-of-Fit	8	2.059	0.2573	1.81	0.095
Pure Error	54	7.664	0.1419		
Total	80	89.827			

The significance level selected for the analysis was 0.05 [42]. Factors with p-values less than 0.05 are statistically significant, and factors with p-values greater than 0.05 are not statistically

significant and do not have any effect on the output, which in this case was surface roughness. From the table, laser energy, hatch distance and the interaction between laser energy and scanning speed have an effect on the surface roughness. The Pareto chart in Figure 9 shows that the pulse energy and hatch distance both have the greatest effect on the roughness, followed by the laser energy.
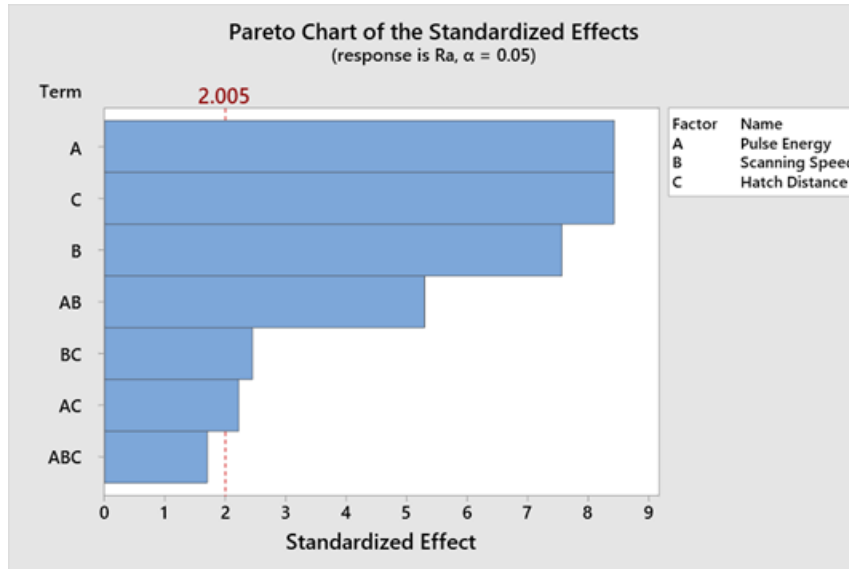
Figure 15: Pareto chart of the standardized effects

The plot in Figure 13a shows that the hatch distance is directly proportional to surface roughness. When the hatch distance is smaller, the degree of overlap between the individual laser tracks increases. An area on the material surface receives more laser pulses, and more material is removed, causing a greater reduction in roughness. A hatch distance too large leaves some portions of the material untouched by the laser in between laser tracks, leaving a minimal reduction in roughness.

It was observed in Figure 13b that the roughness Ra was low with lower scanning speeds, and increased with higher scanning speeds. At slower speeds, the individual laser pulses are closer to each other and overlap, therefore an area on the substrate is exposed to more laser pulses. This

causes more material to be ablated, reducing surface roughness. A high scanning speed increases the distance between the pulses and reduces the number of pulses the material receives per unit area, so the material is not evaporated as desired.

At high pulse energy in Figure 13c, the surface roughness produced is high. At low pulse energy, the roughness values are lower, and at intermediate level of laser pulse, the surface roughness values are at their lowest. Similar results have been observed in other surface improvement studies [43]–[45]. At low pulse energy, the laser only removes a minimal amount of material leaving some peaks on the material surface. The high pulse energy removes a relatively large amount of material per pulse, causing deep grooves on the surfaces, increasing surface roughness.

Optimization of parameters was carried out using statistical software to achieve the optimal process parameters to minimize roughness [46]. The optimized parameters are shown in Figure 12 in red colored text. They are; laser energy of 20 µJ, scanning speed of 5 mm/s, and hatch distance of 10 µm. Under the optimized parameters, a minimum roughness of 3.024 µm can be achieved after the laser ablation process.
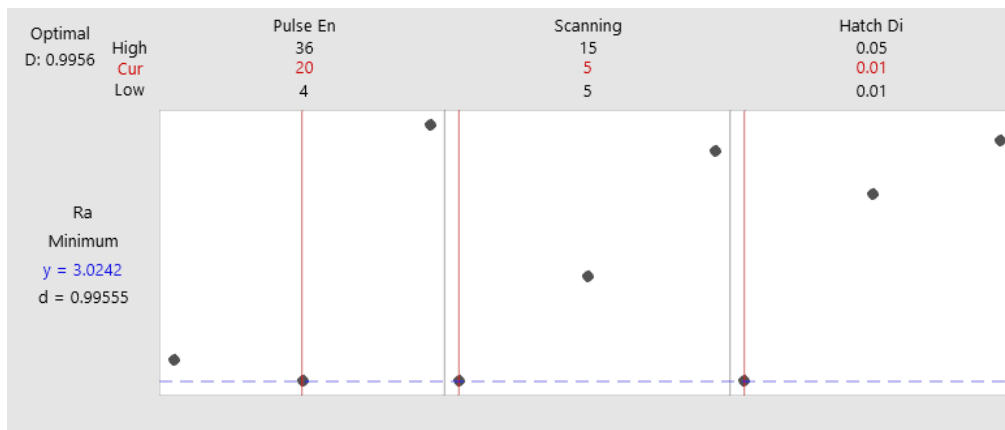
Figure 16: Optimal laser parameters from Minitab
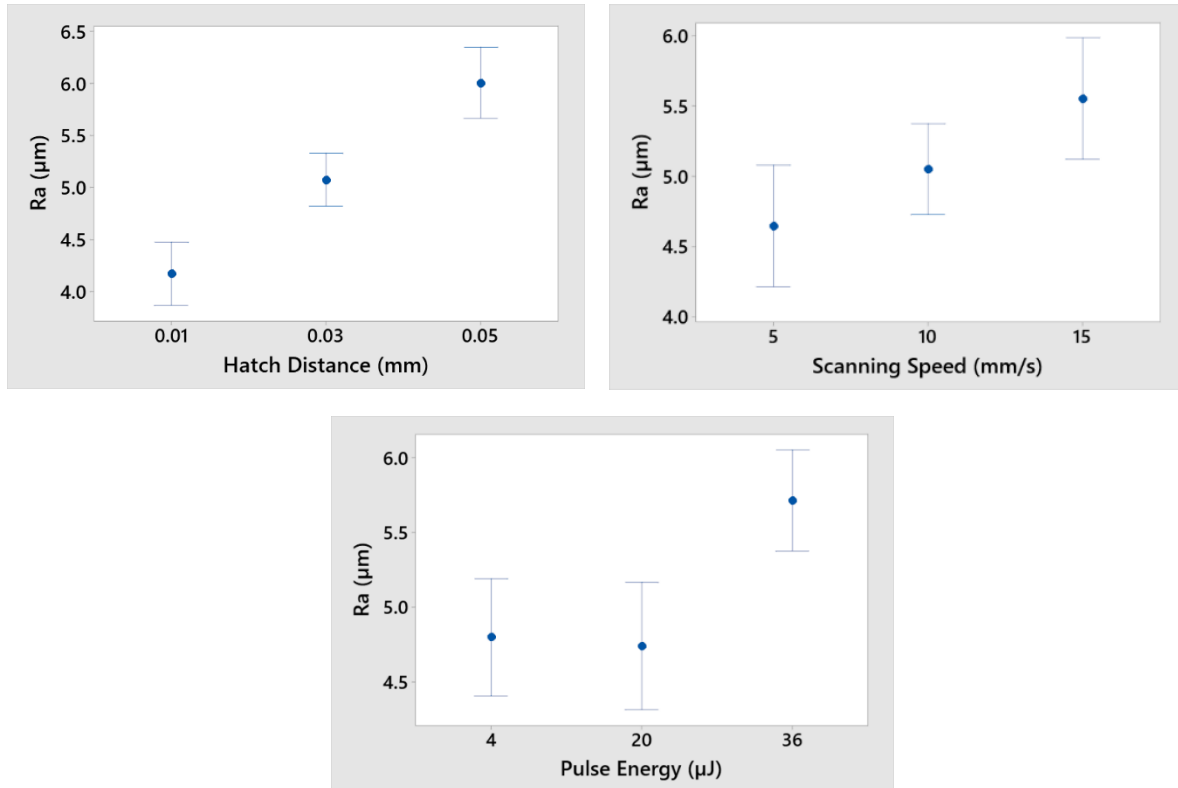
Figure 17: (a) Plot of hatch distance against Ra (b) Plot of scanning speed against Ra (c) Plot of scanning speed against Ra

CNC Grinding

The surface roughness averages of the samples were measured after CNC grinding. The lowest roughness average recorded was Ra of 0.125 µm. An analysis of variance was performed using Minitab Statistical Software to observe the significance of each grinding parameter for each wheel on the surface roughness. A significance level of 0.05 was selected for the analysis. Tables 5 and 6 show the results of the ANOVA.

Table 6: Analysis of Variance for Wheel 1

Source	DF	Adj SS	Adj MS	F-Value	P-Value
Model	3	0.008872	0.002957	63.26	0.000
Linear	2	0.002292	0.001146	24.52	0.000
Workpiece speed	1	0.001302	0.001302	27.85	0.001
Depth of cut	1	0.000990	0.000990	21.18	0.002
2-Way Interactions	1	0.006580	0.006580	140.75	0.000
Workpiece speed*Depth of cut	1	0.006580	0.006580	140.75	0.000
Error	8	0.000374	0.000047		
Total	11	0.009246			

Table 7: Analysis of Variance for Wheel 2

Source	DF	Adj SS	Adj MS	F-Value	P-Value
Model	3	0.106318	0.035439	158.92	0.000
Linear	2	0.054046	0.027023	121.18	0.000
Workpiece speed	1	0.006165	0.006165	27.65	0.001
Depth of cut	1	0.047880	0.047880	214.71	0.000
2-Way Interactions	1	0.052272	0.052272	234.40	0.000
Workpiece speed*Depth of cut	1	0.052272	0.052272	234.40	0.000
Error	8	0.001784	0.000223		
Total	11	0.108102			

The analysis of variance for both wheels shows that all the factors, and the interaction between the factors are statistically significant and influence the surface roughness of the samples.
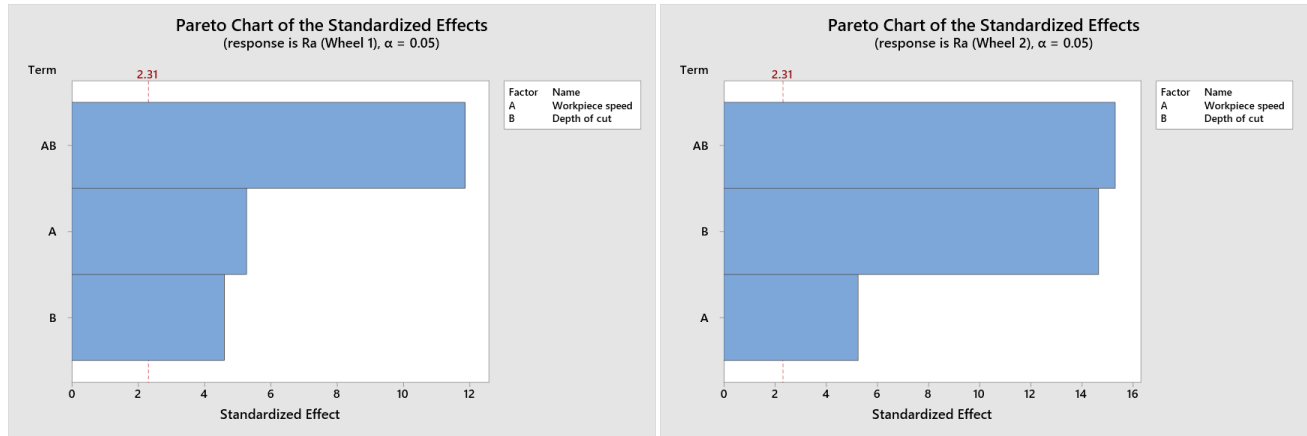
Figure 18: Pareto Chart of Grinding Parameters

It was observed in Figure 14 that the average surface roughness achieved by using Wheel was much lower than Wheel 2.
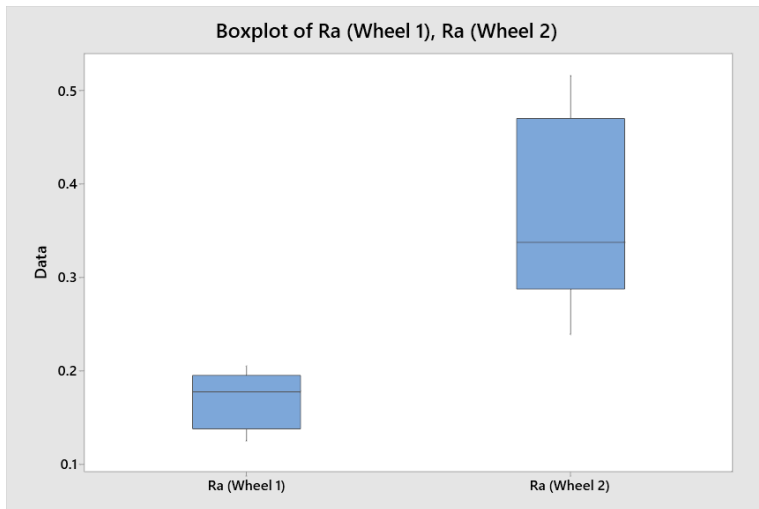
Figure 19: Boxplot of Ra produced by Wheel 1 and Wheel 2

Optimization of parameters was carried out using statistical software to achieve the optimal process parameters to minimize roughness [46]. Only Wheel 1 was considered since it produced a lower roughness. The optimized parameters are shown in Figure 15 in red colored text. They are; workpiece speed of 8.6 m/min and depth of cut of 0.013 mm using Wheel 1. With the optimized parameters, a surface roughness of 0.1283 µm can be achieved.

29

| Optimal
D: 0.9583 | High
Cur
Low | Workpiec
14.70
[8.60]
8.60 | Depth of
0.0250
[0.0130]
0.0130 |

Ra (Whee
Minimum
y = 0.1283
d = 0.95833
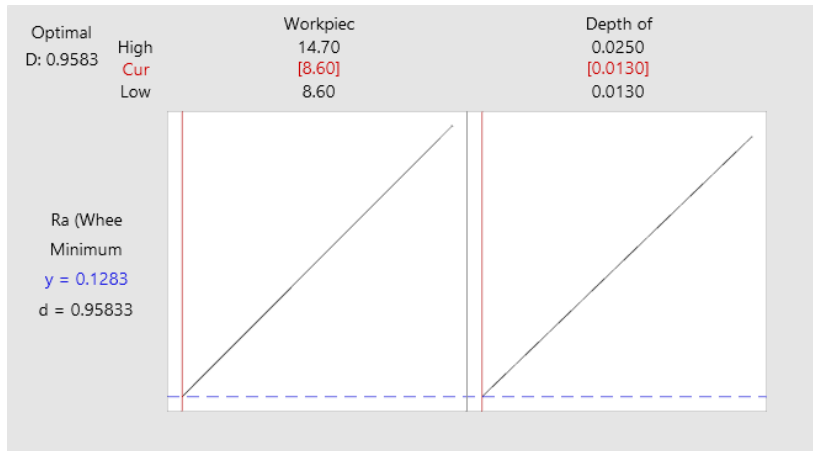
Figure 20: Optimized grinding parameters from Minitab

Microstructure Analysis

SEM images were taken of the as-printed sample after selective laser melting. The samples that had the least surface roughness after each post-processing method were also observed.

| 100 µm | EHT = 2.00 kV | Signal A = SE2 | Date :22 Nov 2022 |
| | WD = 10.7 mm | Mag = 150 X | Sample ID = As printed side |
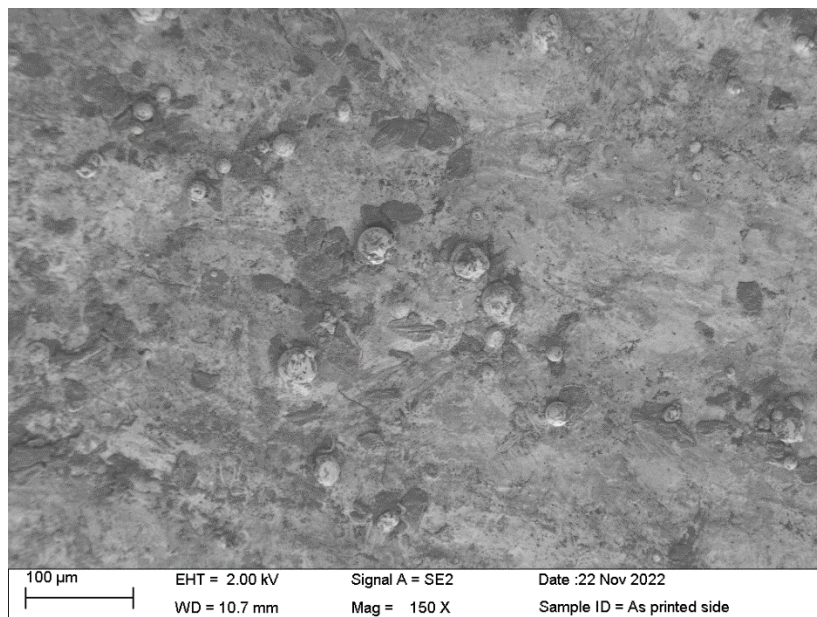
Figure 21: SEM image of Inconel 718 sample after SLM
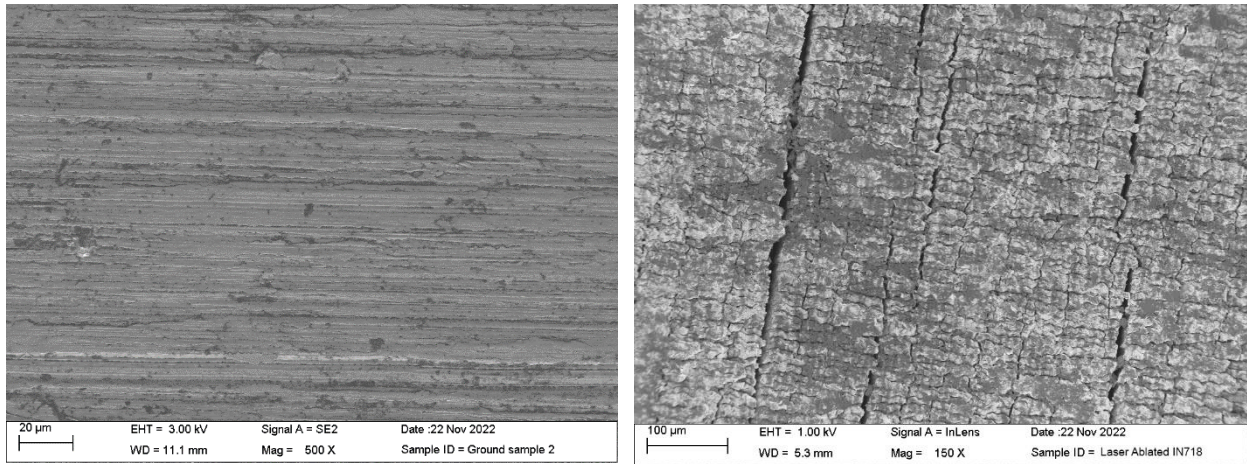
Figure 22: SEM image of Inconel 718 sample after (a) grinding (b) laser ablation

Several un-melted particles were observed across the sample surface after selective laser melting

which contributed to the high surface roughness. After Precision CNC grinding, the surface

appears to be much smoother, and all the defects are removed. After laser ablation, the un-melted

particles were removed, but cracks are present across the surface of the part. This is attributed to

the oxidation of the sample because the laser ablation process was carried out in an open

chamber with no shielding gas. EDS analysis of the samples showed an increase in oxygen

atomic percentage from 12.07% to 61.08% on the sample surface after laser ablation.
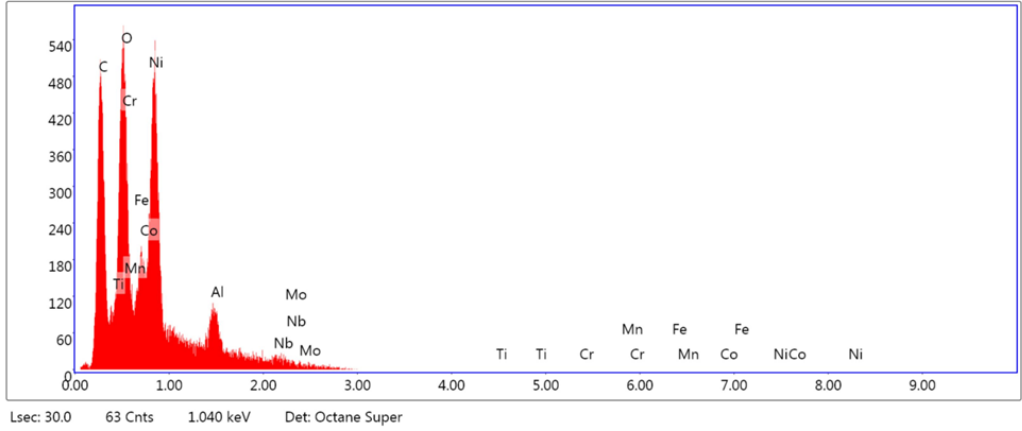
Figure 23: EDS results of as-printed sample

Table 8: Oxygen Composition in as-printed sample surface

Element	Weight %	Atomic %	Net Int.	Error %	Kratio	Z	A	F
O K	14.70	12.07	130.96	14.73	0.1167	0.9546	0.8317	1.0000
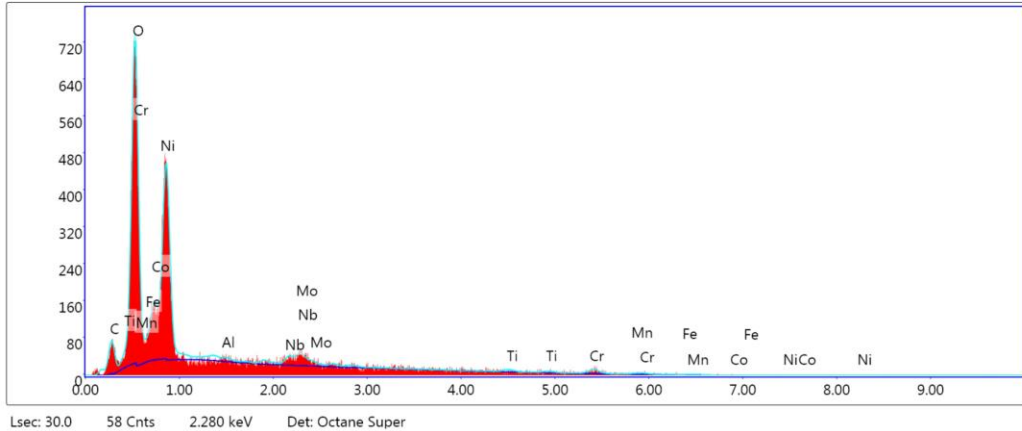
Figure 24: EDS results of laser ablated sample

Table 9: Oxygen composition in laser ablated sample surface

Element	Weight %	Atomic %	Net Int.	Error %	Kratio	Z	A	F
O K	35.89	61.08	436.18	7.47	0.2756	1.1	0.6411	1.0000

Hardness Results

The hardness of the samples was recorded after SLM printing, laser ablation and CNC grinding and the HRD values are shown in the table below. No significant difference was observed between the various samples.

Table 10: Hardness values of samples before and after post-processing.

As-printed samples (HRD)	After Laser Ablation (HRD)	After CNC Grinding (HRD)
42.2	38.8	39.6
44.2	38.8	43.7
45.4	42.1	44.2
42.1	42.8	44.1

CHAPTER V

CONCLUSION

In this study, the laser ablation and precision CNC grinding post-processing techniques were applied to the surface of Inconel 718 samples produced by selective laser melting to observe their effects on the surface properties of the material. For the laser ablation experiments, A 3×3 full factorial experiment was used, with 3 replicates of each combination of the processing parameters. The processing parameters considered were laser energy, scanning speed and hatch distance. The precision CNC grinding experiments were performed using two grinding wheel with different grain size and hardness values with 3 replicates for each combination of grinding process parameters. The parameters that were varied were grinding wheel, workpiece speed, and depth of cut. The surface roughness averages of the samples were measured after both experiments. The optimal processing parameters for each technique were found using statistical analysis with Ra as the performance measure. The microstructures and elemental composition of selected samples were studied using SEM and EDX. The conclusions drawn from the investigation are summarized below:

(1) The precision CNC grinding using a Norton 12-inch diameter Aluminum Oxide grinding wheel with a grit size of 46, H hardness, coarse grade, and vitrified bond with a workpiece speed of 8.6 m/min and a depth of cut 0.013 mm of produced the lowest surface roughness of 0.125 µm.

(2) SEM images showed that the ground sample surface was free of all defects produced by the selective laser melting process. The surface of the laser ablated surface possessed cracks as a result of oxidation.

(3) Oxidation occurred on the surface of the laser ablated samples. EDS analysis showed the increase in oxygen atomic percentage from 12.07% to 61.08%. The reason behind this is the exposure of the samples to the atmosphere during the ablation process. A shielding gas can be employed in future experiments to reduce oxidation.

(4) Laser energy, scanning speed and hatch distance are all significant to the surface roughness of the part after laser ablation. Laser energy set to 20 µJ, scanning speed set to 5 mm/s, and hatch distance set to 10 µm produced a minimum surface roughness of 3.09 µm.

(5) Precision CNC grinding produced a more desirable surface finish and integrity than laser ablation based on the study in this research. Further study is needed to optimize the laser ablation process and/or the grinding process for achieving required surface integrity of additive manufactured Inconel 718 parts with minimum energy use.

REFERENCES

[1]   M. Rahman, W. K. H. Seah, and T. T. Teo, "The machinability of inconel 718," *J Mater Process Technol*, vol. 63, no. 1–3, pp. 199–204, Jan. 1997, doi: 10.1016/S0924-0136(96)02624-6.

[2]   E. O. Ezugwu, Z. M. Wang, and A. R. Machado, "The machinability of nickel-based alloys: a review," *J Mater Process Technol*, vol. 86, no. 1–3, pp. 1–16, Feb. 1999, doi: 10.1016/S0924-0136(98)00314-8.

[3]   C. Y. Yap, C. K. Chua, and Z. L. Dong, "An effective analytical model of selective laser melting," *http://dx.doi.org/10.1080/17452759.2015.1133217*, vol. 11, no. 1, pp. 21–26, Jan. 2016, doi: 10.1080/17452759.2015.1133217.

[4]   G. Strano, L. Hao, R. M. Everson, and K. E. Evans, "Surface roughness analysis, modelling and prediction in selective laser melting," *J Mater Process Technol*, vol. 213, no. 4, pp. 589–597, Apr. 2013, doi: 10.1016/J.JMATPROTEC.2012.11.011.

[5]   E. Wycisk, A. Solbach, S. Siddique, D. Herzog, F. Walther, and C. Emmelmann, "Effects of Defects in Laser Additive Manufactured Ti-6Al-4V on Fatigue Properties," *Phys Procedia*, vol. 56, no. C, pp. 371–378, Jan. 2014, doi: 10.1016/J.PHPRO.2014.08.120.

[6]   S. Sun, M. Brandt, and M. Easton, "Powder bed fusion processes: An overview," *Laser Additive Manufacturing: Materials, Design, Technologies, and Applications*, pp. 55–77, Jan. 2017, doi: 10.1016/B978-0-08-100433-3.00002-6.

[7]   B. Ferrar, L. Mullen, E. Jones, R. Stamp, and C. J. Sutcliffe, "Gas flow effects on selective laser melting (SLM) manufacturing performance," *J Mater Process Technol*, vol. 212, no. 2, pp. 355–364, Feb. 2012, doi: 10.1016/J.JMATPROTEC.2011.09.020.

[8]   S. Sun, M. Brandt, and M. Easton, "Powder bed fusion processes: An overview," *Laser Additive Manufacturing: Materials, Design, Technologies, and Applications*, pp. 55–77, Jan. 2017, doi: 10.1016/B978-0-08-100433-3.00002-6.

[9]   E. Malekipour and H. El-Mounayri, "Common defects and contributing parameters in powder bed fusion AM process and their classification for online monitoring and control: a review," *International Journal of Advanced Manufacturing Technology*, vol. 95, no. 1–4, pp. 527–550, Mar. 2018, doi: 10.1007/S00170-017-1172-6.

[10]   R. J. Smith, M. Hirsch, R. Patel, W. Li, A. T. Clare, and S. D. Sharples, "Spatially resolved acoustic spectroscopy for selective laser melting," *J Mater Process Technol*, vol. 236, pp. 93–102, Oct. 2016, doi: 10.1016/J.JMATPROTEC.2016.05.005.

[11]   J. Ning, D. E. Sievers, H. Garmestani, and S. Y. Liang, "Analytical modeling of part porosity in metal additive manufacturing," *Int J Mech Sci*, vol. 172, p. 105428, Apr. 2020, doi: 10.1016/J.IJMECSCI.2020.105428.

[12]   P. Edwards, A. O'Conner, and M. Ramulu, "Electron beam additive manufacturing of titanium components: Properties and performance," *Journal of Manufacturing Science and Engineering, Transactions of the ASME*, vol. 135, no. 6, Dec. 2013, doi: 10.1115/1.4025773/375746.

[13]   L. N. Carter, C. Martin, P. J. Withers, and M. M. Attallah, "The influence of the laser scan strategy on grain structure and cracking behaviour in SLM powder-bed fabricated nickel

superalloy," *J Alloys Compd*, vol. 615, pp. 338–347, Dec. 2014, doi:

10.1016/J.JALLCOM.2014.06.172.

[14]   P. Mercelis and J. P. Kruth, "Residual stresses in selective laser sintering and selective

laser melting," *Rapid Prototyp J*, vol. 12, no. 5, pp. 254–265, 2006, doi:

10.1108/13552540610707013/FULL/HTML.

[15]   N. J. Harrison, I. Todd, and K. Mumtaz, "Reduction of micro-cracking in nickel

superalloys processed by Selective Laser Melting: A fundamental alloy design approach,"

Acta Mater, vol. 94, pp. 59–68, Aug. 2015, doi: 10.1016/J.ACTAMAT.2015.04.035.

[16]   M. F. Zaeh and G. Branner, "Investigations on residual stresses and deformations in

selective laser melting," *Production Engineering*, vol. 4, no. 1, pp. 35–45, Feb. 2010, doi:

10.1007/S11740-009-0192-Y.

[17]   M. F. Zäh and S. Lutzmann, "Modelling and simulation of electron beam melting,"

Production Engineering, vol. 4, no. 1, pp. 15–23, Feb. 2010, doi: 10.1007/S11740-009-

0197-6.

[18]   J. Kruth, L. Froyen, … J. V. V.-J. of materials, and undefined 2004, "Selective laser

melting of iron-based powder," *Elsevier*, Accessed: Mar. 07, 2022. [Online]. Available:

https://www.sciencedirect.com/science/article/pii/S0924013604002201?casa_token=u78oi

pRqy6IAAAAA:UMauEhH3QbWfM-

oktVbkB3oDPwbNBJP8yxo1s7VXp4XTwbGvz2P4ei1ZATPwjpQOyQNCXftRIX8

[19]   R. Li, J. Liu, Y. Shi, L. Wang, W. J.-T. I. J. of, and undefined 2012, "Balling behavior of

stainless steel and nickel powder during selective laser melting process," *Springer*, vol.

59, no. 9–12, pp. 1025–1035, Apr. 2012, doi: 10.1007/s00170-011-3566-1.

[20] E. Ukar, A. Lamikiz, F. Liébana, S. Martínez, and I. Tabernero, "An industrial approach of laser polishing with different laser sources," *Materwiss Werksttech*, vol. 46, no. 7, pp. 661–667, Jul. 2015, doi: 10.1002/MAWE.201500324.

[21] L. Chen, X. Zhang, Y. Wang, and T. A. Osswald, "Laser polishing of Cu/PLA composite parts fabricated by fused deposition modeling: Analysis of surface finish and mechanical properties," *Polym Compos*, vol. 41, no. 4, pp. 1356–1368, Apr. 2020, doi: 10.1002/PC.25459.

[22] F. Zhihao, L. Libin, C. Longfei, and G. Yingchun, "Laser Polishing of Additive Manufactured Superalloy," *Procedia CIRP*, vol. 71, pp. 150–154, Jan. 2018, doi: 10.1016/J.PROCIR.2018.05.088.

[23] S. Dadbakhsh, L. Hao, and C. Y. Kong, "Surface finish improvement of LMD samples using laser polishing," *https://doi.org/10.1080/17452759.2010.528180*, vol. 5, no. 4, pp. 215–221, Dec. 2010, doi: 10.1080/17452759.2010.528180.

[24] H. Guoqing, S. Yang, and G. Yingchun, "Tailoring metallic surface properties induced by laser surface processing for industrial applications," *Nanotechnology and Precision Engineering*, vol. 2, no. 1, p. 29, Dec. 2020, doi: 10.1016/J.NPE.2019.03.003.

[25] B. Yilbas, S. Akhtar, C. K.-O. and L. in Engineering, and undefined 2010, "Laser surface treatment of Inconel 718 alloy: thermal stress analysis," *Elsevier*, Accessed: Mar. 07, 2022. [Online]. Available: https://www.sciencedirect.com/science/article/pii/S0143816610000552?casa_token=OGo qF8114WMAAAAA:I9aQ9j9S2999U8Lug-HZtdYuBtzvTnixkirJshbH8V-48Z0KmAeKzPqDA1QRvGOqJewwKukQ6oc

[26]   B. S. Yilbas, H. Ali, N. Al-Aqeeli, and C. Karatas, "[INVITED] Laser treatment of
       Inconel 718 alloy and surface characteristics," *Opt Laser Technol*, vol. 78, pp. 153–158,
       Apr. 2016, doi: 10.1016/J.OPTLASTEC.2015.11.006.

[27]   Y. Li, Z. Zhang, and Y. Guan, "Thermodynamics analysis and rapid solidification of laser
       polished Inconel 718 by selective laser melting," *Appl Surf Sci*, vol. 511, p. 145423, May
       2020, doi: 10.1016/J.APSUSC.2020.145423.

[28]   X. Liu, D. Du, and G. Mourou, "Laser ablation and micromachining with ultrashort laser
       pulses," *IEEE J Quantum Electron*, vol. 33, no. 10, pp. 1706–1716, Oct. 1997, doi:
       10.1109/3.631270.

[29]   K. H. Leitz, B. Redlingshöer, Y. Reg, A. Otto, and M. Schmidt, "Metal Ablation with
       Short and Ultrashort Laser Pulses," *Phys Procedia*, vol. 12, no. PART 2, pp. 230–238,
       Jan. 2011, doi: 10.1016/J.PHPRO.2011.03.128.

[30]   A. Mohammad, M. K. Mohammed, and A. M. Alahmari, "Effect of laser ablation
       parameters on surface improvement of electron beam melted parts," *The International
       Journal of Advanced Manufacturing Technology 2016 87:1*, vol. 87, no. 1, pp. 1033–
       1044, Mar. 2016, doi: 10.1007/S00170-016-8533-4.

[31]   S. L. Campanelli, G. Casalino, N. Contuzzi, and A. D. Ludovico, "Taguchi Optimization
       of the Surface Finish Obtained by Laser Ablation on Selective Laser Molten Steel Parts,"
       Procedia CIRP, vol. 12, pp. 462–467, Jan. 2013, doi: 10.1016/J.PROCIR.2013.09.079.

[32]   J. Kruth, E. Yasa, J. D.-P. of the 3rd international, and undefined 2008, "Roughness
       improvement in selective laser melting," *lirias.kuleuven.be*, Accessed: Nov. 23, 2021.
       [Online]. Available: https://lirias.kuleuven.be/retrieve/117846

[33]   J. Kopac and P. Krajnik, "High-performance grinding—A review," *J Mater Process Technol*, vol. 175, no. 1–3, pp. 278–284, Jun. 2006, doi: 10.1016/J.JMATPROTEC.2005.04.010.

[34]   F. Klocke *et al.*, "Abrasive machining of advanced aerospace alloys and composites," *CIRP Annals*, vol. 64, no. 2, pp. 581–604, Jan. 2015, doi: 10.1016/J.CIRP.2015.05.004.

[35]   "What is Surface Grinding? – Surface Grinding Machine." https://surfacegrindingmachine.wordpress.com/2017/03/06/what-is-surface-grinding/ (accessed Dec. 06, 2022).

[36]   P. L. Tso, "Study on the grinding of Inconel 718," *J Mater Process Technol*, vol. 55, no. 3–4, pp. 421–426, Dec. 1995, doi: 10.1016/0924-0136(95)02026-8.

[37]   M. Novák, N. Náprstková, and J. Józwik, "Analysis of the surface profile and its material share during the grinding inconel 718 alloy," *Advances in Science and Technology Research Journal*, vol. 9, no. Vol. 9, nr 26, pp. 41--48, 2015, doi: 10.12913/22998624/2363.

[38]   J. Wang, J. Xu, X. Wang, X. Zhang, X. Song, and X. Chen, "A comprehensive study on surface integrity of nickel-based superalloy Inconel 718 under robotic belt grinding," *https://doi.org/10.1080/10426914.2018.1512137*, vol. 34, no. 1, pp. 61–69, Jan. 2018, doi: 10.1080/10426914.2018.1512137.

[39]   C. F. Yao, Q. C. Jin, X. C. Huang, D. X. Wu, J. X. Ren, and D. H. Zhang, "Research on surface integrity of grinding Inconel718," *The International Journal of Advanced Manufacturing Technology 2012 65:5*, vol. 65, no. 5, pp. 1019–1030, Jun. 2012, doi: 10.1007/S00170-012-4236-7.

[40]   A. K. Srivastava and R. Pavel, "Grinding investigations of Ti-6Al-4V parts produced using direct metal laser sintering technology," *International Journal of Mechatronics and Manufacturing Systems*, vol. 8, no. 5–6, pp. 223–242, 2015, doi: 10.1504/IJMMS.2015.073566.

[41]   D. Curtis, H. Krain, A. Winder, and D. Novovic, "Impact of grinding wheel specification on surface integrity and residual stress when grinding Inconel 718:," *https://doi.org/10.1177/0954405420961209*, vol. 235, no. 10, pp. 1668–1681, Oct. 2020, doi: 10.1177/0954405420961209.

[42]   D. Montgomery, *Design and analysis of experiments*. 2017. Accessed: Nov. 26, 2021. [Online]. Available: https://books.google.com/books?hl=en&lr=&id=Py7bDgAAQBAJ&oi=fnd&pg=PA1&dq =design+and+analysis+of+experiments&ots=X7s6l2NQ26&sig=ni9tOcnFEhGKwhV6kje oOpYHstY

[43]   T. L. Perry, D. Werschmoeller, X. Li, F. E. Pfefferkorn, and N. A. Duffie, "Pulsed laser polishing of micro-milled Ti6Al4V samples," *J Manuf Process*, vol. 11, no. 2, pp. 74–81, Jul. 2009, doi: 10.1016/J.JMAPRO.2009.10.001.

[44]   T. L. Perry, D. Werschmoeller, N. A. Duffie, X. Li, and F. E. Pfefferkorn, "Examination of selective pulsed laser micropolishing on microfabricated nickel samples using spatial frequency analysis," *Journal of Manufacturing Science and Engineering, Transactions of the ASME*, vol. 131, no. 2, pp. 0210021–0210029, Apr. 2009, doi: 10.1115/1.3075874/468477.

[45]   T. A. Mai and G. C. Lim, "Micromelting and its effects on surface topography and properties in laser polishing of stainless steel," *J Laser Appl*, vol. 16, no. 4, p. 221, Dec. 2004, doi: 10.2351/1.1809637.

[46]   A. Alin, "Minitab," *Wiley Interdiscip Rev Comput Stat*, vol. 2, no. 6, pp. 723–727, Nov. 2010, doi: 10.1002/WICS.113.

BIOGRAPHICAL SKETCH

Sampson K. Canacoo acquired his bachelor's degree in Mechanical Engineering from the Kwame Nkrumah University of Science and Technology in Ghana in 2019. He joined the Manufacturing and Industrial Engineering department at the University of Texas Rio Grande Valley and graduated with a Master of Science in Manufacturing Engineering in December 2022. He was awarded the Presidential Graduate Research Assistantship and worked as a research and teaching assistant under Dr. Anil Srivastava. Sampson can be reached at samcanac.96@gmail.com.